symmetry

IMPACT FACTOR 2.2

CITESCORE 5.3

Article

Asymmetry in the Mean Free Path of Neutrinos in Hot Neutron Matter Under Strong Magnetic Fields

Eduardo Bauer and Vanesa D. Olivera

Special Issue

Neutrino Physics and Symmetries

Edited by

Prof. Dr. Eduardo Bauer, Dr. Floyd W. Stecker and Prof. Dr. Jiajie Ling

MDPI

https://doi.org/10.3390/sym17060896

symmetry

MDPI

Article

Asymmetry in the Mean Free Path of Neutrinos in Hot Neutron Matter Under Strong Magnetic Fields

Eduardo Bauer [1,2,*] and Vanesa D. Olivera [2]

[1] Institute of Physics, IFLP-CONICET, diag 113 e/63-64, La Plata 1900, Argentina
[2] Facultad de Ciencias Astronómicas y Geofísicas, Paseo del Bosque s/n, La Plata 1900, Argentina
* Correspondence: bauer@fisica.unlp.edu.ar

Abstract: We investigate the asymmetry in the mean free path of massive neutrinos propagating through hot neutron matter under strong magnetic fields. The system is studied at temperatures up to 30 MeV and baryon densities up to $\rho/\rho_0 = 2.5$, where ρ_0 is the nuclear saturation density. Magnetic field strengths up to $B = 10^{18}$ G are considered. We analyze three different equations of state: one corresponding to a non-interacting Fermi gas and two derived from Skyrme-type interactions. The impact of a finite neutrino mass is assessed and found to be negligible within the energy range considered. The neutrino mean free path is computed for various angles of incidence with respect to the magnetic field direction, revealing a clear angular asymmetry. We show that quantum interference terms contribute significantly to this asymmetry, enhancing neutrino emission in directions perpendicular to the magnetic field at high densities. This result contrasts with previous expectations and suggests a revised interpretation of neutrino transport in magnetized nuclear matter.

Keywords: a Asymmetry in the neutrino mean free path; equation of state of stellar matter; the pulsar kick problem; impact of neutrino oscillations

Academic Editor: Alberto Ruiz-Jimeno

Received: 28 April 2025
Revised: 28 May 2025
Accepted: 4 June 2025
Published: 6 June 2025

Citation: Bauer, E.; Olivera, V.D. Asymmetry in the Mean Free Path of Neutrinos in Hot Neutron Matter Under Strong Magnetic Fields. *Symmetry* **2025**, *17*, 896. https://doi.org/10.3390/sym17060896

1. Introduction

Neutrino oscillation is a quantum mechanical phenomenon in which neutrinos change their flavor (electron, muon, or tau) as they propagate through space. This behavior demonstrates that neutrinos have mass, a fact that challenges the Standard Model of particle physics, which initially assumed massless neutrinos. The discovery of neutrino oscillations was first conclusively demonstrated through the observation of atmospheric neutrinos by the Super–Kamiokande experiment. In 1998, the Super–Kamiokande collaboration reported a deficit in the expected number of muon neutrinos arriving from the atmosphere, depending on the distance traveled, providing strong evidence for oscillation and therefore non-zero neutrino mass [1]. This groundbreaking result has profound implications: it not only necessitates an extension of the Standard Model but also opens new avenues in cosmology and particle physics, including the role of neutrinos in the evolution of the universe and the search for CP violation in the lepton sector, among other areas.

The confirmation that neutrinos have mass and oscillate between flavors has significantly deepened our understanding of their role in astrophysical environments, especially in extreme conditions such as those found in neutron stars and magnetars. These ultra-dense stellar remnants, particularly magnetars, whose magnetic fields can reach surface intensities of 10^{14}–10^{15} G and increase dramatically within their dense interiors [2], provide natural laboratories for studying neutrino behavior under intense magnetic forces. In such

environments, neutrino emission becomes a dominant cooling mechanism and influences the star's thermal and magnetic evolution [3]. Within the broader context of core-collapse supernovae, the review by Burrows and Vartanyan [4] provides a comprehensive overview of the problem, addressing not only neutrino physics but also the evolution of the supernova remnant. Moreover, the strong magnetic fields in magnetars can affect neutrino propagation and oscillation patterns, potentially leading to flavor conversions enhanced by matter and magnetic effects [5–8]. Understanding neutrino interactions in these settings is crucial not only for modeling supernovae and neutron star formation but also for probing the physics of dense matter, magnetic field generation, and the potential existence of sterile neutrinos or non-standard interactions beyond the Standard Model [9]. Thus, the study of neutrino oscillations not only reshapes fundamental particle physics but also enriches our comprehension of the most violent and enigmatic objects in the cosmos.

One particularly intriguing astrophysical phenomenon potentially linked to neutrino behavior in highly magnetized neutron stars is the so-called pulsar kick: the observation that many pulsars are born with high space velocities, often exceeding 1000 km/s, far greater than those of their progenitor stars [10]. While several mechanisms have been proposed, one compelling explanation involves anisotropic neutrino emission during the proto-neutron star cooling phase, especially in the presence of ultra-strong magnetic fields. These fields can polarize the medium, thus modifying the cross-sections for neutrino interactions, resulting in asymmetric momentum transfer that imparts a net recoil to the newly formed neutron star [11]. Magnetars, with their extreme field strengths, provide a natural context in which such asymmetries could be amplified. Furthermore, certain models suggest that parity-violating weak interactions in a magnetized medium could generate directional neutrino fluxes aligned with the magnetic axis [12]. These processes offer a viable channel for generating the observed natal kicks and connect large-scale neutron star dynamics with microphysical processes occurring under extreme conditions, thus linking compact object astrophysics with fundamental particle interactions.

In this work, we focus on the inelastic scattering of neutrinos with neutrons, a mechanism responsible for the asymmetric emission of neutrinos. More specifically, we evaluate the neutrino mean free path (defined as the inverse of the total neutrino cross section per unit volume) in hot, dense matter under the influence of a strong magnetic field. The neutrino mass is very small, $m_\nu \lesssim 1$ eV, and this non-zero mass allows for the presence of a right-handed component in the neutrino state, although its contribution is expected to be negligible. In the limiting case of massless neutrinos, only fully polarized left-handed neutrinos exist. These represent the dominant contribution and are the main focus of this work. Nevertheless, to gain some insight into the physics of right-handed neutrinos, we also discuss this point.

It is worth mentioning that we have previously studied the mean free path of left-handed neutrinos in Ref. [13], where a specific set of approximations was employed. In the present work, we revisit these approximations, which leads to the emergence of quantum interference terms that were not considered before.

The neutrino–neutron inelastic scattering cross section can be evaluated either in free space or within a dense medium. However, the mean free path is physically meaningful only in a dense medium, which must be characterized by an equation of state (EoS). In this work, we explore three different equations of state. The first one assumes no strong interaction among neutrons, whereas the remaining two are based on the Hartree–Fock approximation employing the Skyrme interaction, commonly known as the Skyrme model.

The neutrino mean free path in the absence of a magnetic field has been studied by many authors using various approximation schemes and models of the trapping environment (see, e.g., Refs. [14–27], and references therein). The behavior of neutrinos in dense

matter under strong magnetic fields has also been explored in the literature [13,28–40]. However, the asymmetry in neutrino emission caused by the breaking of isotropy due to the magnetic field has not been extensively discussed.

This paper is organized as follows: In Section 2, we briefly discuss neutrino polarization. In Section 3, we present elements of the EoS and derive an analytical expression for the neutrino cross section per unit volume for left-handed neutrinos. In Section 4, we discuss our results, and finally, in Section 5, we present our conclusions.

2. Neutrino Polarization: A Brief Discussion

The existence of a nonzero neutrino mass has profound implications for the structure of neutrino states. In the massless limit, neutrinos are purely left-handed and antineutrinos are right-handed, as dictated by the Standard Model. However, once a mass term is introduced, each neutrino state acquires both left- and right-helicity components due to the Lorentz structure of the Dirac spinor. The right-helicity component of a neutrino (or left-helicity component of an antineutrino) becomes nonzero, but its amplitude is suppressed by a factor proportional to m_ν / E_ν, where m_ν is the neutrino mass and E_ν its energy. Given the extremely small mass of the neutrino compared to typical energies involved, the right-helicity component is extremely suppressed and often considered unobservable. Nonetheless, its existence is a direct consequence of neutrino mass and can, in principle, be probed in precision experiments involving polarized sources or detectors.

In principle, the presence of both helicity components in a massive neutrino state opens the possibility of helicity oscillations, especially when neutrinos propagate through external fields or media. These transitions between left- and right-helicity states are suppressed in vacuum due to the smallness of the mass, but can be enhanced in certain conditions, such as in the presence of strong magnetic fields or dense matter through mechanisms involving spin-flip processes or magnetic moment interactions [41–44]. Despite their tiny amplitude, right-helicity neutrino components could have significant implications in astrophysical environments, where long propagation distances and extreme conditions might lead to cumulative effects. Moreover, if right-handed neutrinos are sterile, i.e., non-interacting under the Standard Model forces, the conversion of active left-handed neutrinos into sterile right-handed states could impact neutrino fluxes observed in experiments and cosmological observables. Thus, even a seemingly negligible component may play a crucial role in scenarios beyond the Standard Model.

Unfortunately, the interaction between right-handed neutrinos and neutrons is not known. Within the framework of the Standard Model, such an interaction is strictly absent, implying a vanishing cross section for right-handed neutrinos. However, as we shall discuss below, the presence of a mass term leads to energy eigenstates that are admixtures of left- and right-handed components. This mixing induces a small correction to the left-handed component, even in states initially produced as purely left-handed. As a result, the modified wave function can exhibit a suppressed but nonzero sensitivity to phenomena that would otherwise involve only right-handed neutrinos. This subtle effect, though minute, forms the basis for exploring possible deviations from Standard Model predictions in neutrino scattering and propagation.

In a more specific way, if the mass of the neutrino is nonzero, then the energy eigenstates are not eigenstates of chirality. The energy eigenstates can be written as a linear combination of left- and right-chiral states through a unitary transformation:

$$|\nu^+\rangle = \cos\theta\,|\nu^L\rangle - \sin\theta\,|\nu^R\rangle, \quad (1)$$

$$|\nu^-\rangle = \sin\theta\,|\nu^L\rangle + \cos\theta\,|\nu^R\rangle, \quad (2)$$

where $|\nu^{+\,(-)}\rangle$ is the positive (negative) energy eigenstate, and $|\nu^{L\,(R)}\rangle$ denotes the left- (right-) chiral component of the neutrino.

In the limiting case of massless neutrinos, $\theta \to 0$, and we recover the following:

$$|\nu^{+}\rangle \to |\nu^{L}\rangle,$$

as expected, since helicity and chirality coincide for massless fermions.

The mixing angle θ is given by the following:

$$\sin\theta = \frac{m_\nu}{\sqrt{E_\nu^2 + m_\nu^2}}, \qquad \cos\theta = \frac{E_\nu}{\sqrt{E_\nu^2 + m_\nu^2}}. \tag{3}$$

Let us focus on Equation (1). The right-chiral component corresponds to a sterile neutrino, whose interactions with a neutron (or other Standard Model particles) are highly suppressed or unknown. Therefore, when calculating the neutrino–neutron cross section, only the left-chiral component contributes. However, due to the nonzero neutrino mass, the left-chiral component is multiplied by a factor $\cos\theta$, reflecting the admixture of the sterile (right-chiral) component. The importance of this correction depends directly on the energy of the neutrino: the smaller the energy, the larger the deviation from a pure left-chiral state.

3. The Neutrino Mean Free Path for a Polarized System

In this section, we present analytical expressions for the mean free path (λ) of left-handed neutrinos in the reaction,

$$\nu + n \to \nu' + n', \tag{4}$$

where ν (ν') and n (n') denote the initial (final) neutrino and neutron, respectively. Specifically, we compute the total cross section per unit volume (σ/V), from which the neutrino mean free path is straightforwardly obtained as

$$\lambda = (\sigma/V)^{-1}. \tag{5}$$

First, we introduce some elements of the equation of state (EoS) employed in this work, where the magnetic field induces spin polarization in the neutron medium. For clarity, the reader is advised that the term "polarization" in Section 2 refers to neutrino helicity, whereas in this section, it pertains to neutron spin polarization. This brief description of the EoS sets the stage for the subsequent discussion, and then we derive the expressions for the cross section per unit volume.

3.1. The EoS Model for Pure Hot Neutron Matter in a Strong Magnetic Field

Our system consists of pure hot neutron matter in a strong magnetic field. To describe it, we employ an equation of state (EoS) derived from the Skyrme model. We also employ a non-interacting Fermi gas EoS, which is simply obtained from the former by putting the strong interaction equal to zero. Due to the presence of the magnetic field, the system becomes polarized. A system of spin-polarized neutron matter consists of an infinite collection of neutrons categorized into two groups based on their spin orientation: those with spin-up and those with spin-down. Their respective number densities are denoted as $\rho_{n,s_n=+1}$ and $\rho_{n,s_n=-1}$, where s_n represents the spin projection. The total number density of the system is then given by

$$\rho_n = \rho_{n,s_n=+1} + \rho_{n,s_n=-1} \tag{6}$$

The degree of spin polarization in the system is quantified by the spin asymmetry density, defined as

$$W_n = \rho_{n,s_n=+1} - \rho_{n,s_n=-1}. \tag{7}$$

A system with $W_n = 0$ corresponds to an unpolarized neutron matter state, where spin-up and spin-down neutrons are equally distributed. On the other hand, when W_n reaches its extreme values of ρ_n or $-\rho_n$, all neutrons are aligned in the same direction, resulting in a completely spin-polarized state: either all spin-up or all spin-down. Intermediate cases, where W_n takes values between these two extreme values, represent states of partial spin polarization.

The equation of state (EoS) is evaluated within the Skyrme model, which provides an effective framework for describing nuclear interactions [45]. This model consists of a two-body contact potential along with additional terms that explicitly depend on density, accounting for the effects of three-body and multi-body forces. By employing this interaction within the Hartree–Fock approximation, one constructs an energy density functional and subsequently the Helmholtz potential. Minimizing this potential determines the physical state of the system. This approach captures the competition between the magnetic field, which promotes alignment of spins along its axis, and the Pauli exclusion principle, which drives the populations $\rho_{n,s_n=+1}$ and $\rho_{n,s_n=-1}$ toward equilibrium. The resulting compromise leads to a state of partial spin polarization, quantified by W_n. The corresponding single-particle spectrum can be written in a form where the interaction gives rise to two distinct contributions: the effective mass and the residual potential energy.

To compute the equation of state (EoS), the required inputs are the total baryon density ρ_n, the temperature T, and the strength of a uniform magnetic field aligned along the z-axis. The resulting outputs are the chemical potential μ_n, the single-particle energy, and the spin-resolved number densities ρ_{n,s_n}. In our framework, the chemical potential is spin-independent, while the number density varies with spin projection.

We now introduce some definitions used throughout this work. First, the function $f_{s_n}(E_n, T)$, which in the thermal equilibrium is given by the Fermi–Dirac particle distribution function:

$$f_{s_n}(E_n, T) = \frac{1}{1 + \exp[(E_n - \mu_n)/T]}\,, \tag{8}$$

where E_n is the neutron single-particle energy and μ_n its chemical potential. The expression for the number density with a defined spin projection is

$$\rho_{n,\,s_n} = \frac{1}{(2\pi)^3} \int d\vec{p}_n \; f(E_{s_n}, T), \tag{9}$$

where $\vec{p}_n$, is the momentum carried by the neutron.

Before concluding this section, we introduce the expression for the spin asymmetry parameter A_n,

$$A_n = \frac{\rho_{n,s_n=+1} - \rho_{n,s_n=-1}}{\rho_{n,s_n=+1} + \rho_{n,s_n=-1}}. \tag{10}$$

This parameter quantifies the polarization level of the system and plays a key role in specifying the initial wave function. For later convenience, we define the following auxiliary quantities:

$$\begin{aligned} \delta_{s_{n\uparrow}} &\equiv \frac{1+s_n}{2}, & \delta_{s_{n\downarrow}} &\equiv \frac{1-s_n}{2}, \\ a_{s_n\uparrow} &\equiv \sqrt{\frac{1+A_n}{2}}\left(\frac{1+s_n}{2}\right) \quad \text{and} \quad a_{s_n\downarrow} \equiv \sqrt{\frac{1-A_n}{2}}\left(\frac{1-s_n}{2}\right), \end{aligned} \tag{11}$$

An up arrow (down arrow) indicates spin up (down), that is, $s_n = +1$ ($s_n = -1$). A more detailed treatment can be found in [46,47].

3.2. The Neutrino Cross Section for a Polarized System

In this section, we present expressions for the left-handed neutrino cross section per unit volume in a polarized system for the inelastic neutrino–neutron reaction. This derivation differs from the one in [13], where we analyzed the same reaction with some approximations. In [13], we split the cross section into two contributions: one for an initial neutron with spin up and the other with spin down. In the present work, we consider a mixed initial neutron wave function, including both spin-up and spin-down components. This wave function is constructed to match the polarization of the entire system. More explicitly, using the initial neutron spin wave function from Equation (A3) in Appendix A, we obtain

$$\langle U_n|\hat{S}_z|U_n\rangle = A_n \frac{\hbar}{2}, \tag{12}$$

where the value of A_n is taken from the EoS.

The employment of this mixed spin wave function results in quantum interference terms that were not considered in [13] and are discussed at the end of this section. Moreover, we establish a self-consistent link between the evaluation of the EoS and the cross section.

Using the Fermi Golden Rule (see, e.g., [48]), we can write down the contribution of the reaction (4), to the total cross section per unit volume simply as follows:

$$\begin{aligned}\frac{\sigma(p_\nu)}{V} &= \int \frac{d\vec{p}_{\nu'}}{(2\pi)^3}\int \frac{d\vec{p}_n}{(2\pi)^3}\int \frac{d\vec{p}_{n'}}{(2\pi)^3}(2\pi)^4\delta^{(4)}(p_\nu + p_n - p_{\nu'} - p_{n'}) \\ &\quad \times f_{s_n}(E_n,T)(1-f_{s_{n'}}(E_{n'},T))\frac{\langle|\mathcal{M}_{\nu'n',\nu n}|^2\rangle}{2^4 E_\nu E_{\nu'} E_n E_{n'}}\,,\end{aligned} \tag{13}$$

where $p_i = (E_i, \vec{p}_i)$ is the four-momentum of particle i, and $\mathcal{M}_{\nu'n',\nu n}$ is the so-called Møller invariant transition matrix, which we define below. The symbol $\langle\ \rangle$ denotes the sum over final states and an average over the initial ones. An important aspect of our scheme is that the use of Equations (A1) and (A6), for the initial neutron and neutrino, implies that we do not perform any averaging over the initial neutrino state or over the initial spin state of the neutron, as both are assumed to be known by hypothesis.

The two ingredients required to obtain the total neutrino cross section are the invariant transition matrix $\mathcal{M}_{\nu'n',\nu n}$ and a model for the equation of state (EoS) of neutron matter. The former describes a two-body process mediated by the weak interaction, while the latter characterizes the state of the strongly interacting neutron system, as previously discussed. We now focus on the evaluation of the matrix $\mathcal{M}_{\nu'n',\nu n}$. Below, we outline the main steps in its derivation; for further details, we refer the reader to [13].

Our starting point is the following Lagrangian density, written in terms of a current–current interaction:

$$\mathcal{L} = \frac{1}{\sqrt{2}} G_F \left(\bar{\psi}_{\nu'}\gamma^\mu(1-\gamma_5)\psi_\nu\right)\left(\bar{\psi}_{n'}\gamma_\mu(C_V - C_A\gamma_5)\psi_n\right). \tag{14}$$

Here, $G_F \simeq 1.436 \times 10^{-49}$ erg cm^{-3} is the Fermi coupling constant, and the coefficients $C_V = -1/2$ and $C_A = -1.23/2$ are the vector and axial-vector couplings, respectively. This expression can be employed only for left-handed neutrinos (or right-handed antineutrinos). For simplicity, we neglect the weak magnetism term, as it is of order $\mathcal{O}(1/m)$ [24,49,50].

The matrix element $\mathcal{M}_{\nu' n', \nu n}$ can be derived from the Lagrangian density above as follows:

$$\mathcal{M}_{\nu' n', \nu n} = \frac{1}{\sqrt{2}} G_F \left(\overline{u}_{\nu'} \gamma^{\mu} (1 - \gamma_5) u_{\nu} \right) \left(\overline{u}_{n'} \gamma_{\mu} (C_V - C_A \gamma_5) u_n \right) . \tag{15}$$

It is convenient to express the squared matrix element as a contraction between a leptonic ($l^{\mu\alpha}$) and a hadronic ($H_{\mu\alpha}$) rank-two tensor:

$$|\mathcal{M}_{\nu' n', \nu n}|^2 = \frac{1}{2} G_F^2 \, l^{\mu\alpha} H_{\mu\alpha} \, , \tag{16}$$

with

$$l^{\mu\alpha} = \left(\overline{u}_{\nu} \gamma^{\mu} (1 - \gamma_5) u_{\nu'} \right) \left(\overline{u}_{\nu'} \gamma^{\alpha} (1 - \gamma_5) u_{\nu} \right), \tag{17}$$

and

$$H_{\mu\alpha} = \left(\overline{u}_{n} (C_V + C_A \gamma_5) \gamma_{\mu} u_{n'} \right) \left(\overline{u}_{n'} \gamma_{\alpha} (C_V - C_A \gamma_5) u_n \right) . \tag{18}$$

The analytical evaluation of Equation (16) is laborious but straightforward. In what follows, we present its non-relativistic reduction, where we employ the spinors given in Equations (A3), (A4), (A7), and (A9). First, we introduce the notation

$$\langle |\mathcal{M}_{\nu' n', \nu n}|^2 \rangle \equiv Tr_{s_n, s_{n'}}(\theta_{\nu}, \theta_{\nu'}, \phi_{\nu'}) \, + \, \Delta Tr_{s_n, s_{n'}}(\theta_{\nu}, \theta_{\nu'}, \phi_{\nu'}), \tag{19}$$

where θ_{ν} ($\theta_{\nu'}$) is the polar angle of the incoming (outgoing) neutrino measured with respect to the direction of the magnetic field (taken along the $\hat{z}$-axis). Here, $\phi_{\nu'}$ is the azimuthal angle of the outgoing neutrino, and without loss of generality, we set $\phi_{\nu} = 0$ for the incoming neutrino. For left-handed neutrinos (or right-handed antineutrinos), we have

$$\begin{aligned}
Tr^{L}_{s_n, s_{n'}}(\theta_{\nu}, \theta_{\nu'}, \phi_{\nu'}) &= 16 E_{\nu} E_{\nu'} m_n^2 \{ C_V^2 \, (1 + \cos\theta_{\nu,\nu'}) (a^2_{s_n\uparrow} \delta_{s_{n'\uparrow}} + a^2_{s_n\downarrow} \delta_{s_{n'\downarrow}}) \\
&+ 2 C_V C_A \, (\cos\theta_{\nu} + \cos\theta_{\nu'}) (a^2_{s_n\uparrow} \delta_{s_{n'\uparrow}} - a^2_{s_n\downarrow} \delta_{s_{n'\downarrow}}) \\
&+ C_A^2 \, [(1 + \cos\theta_{\nu} \cos\theta_{\nu'} - \sin\theta_{\nu} \sin\theta_{\nu'} \cos\phi_{\nu'}) (a^2_{s_n\uparrow} \delta_{s_{n'\uparrow}} + a^2_{s_n\downarrow} \delta_{s_{n'\downarrow}}) \\
&+ 2(1 - \cos\theta_{\nu} + \cos\theta_{\nu'} - \cos\theta_{\nu} \cos\theta_{\nu'}) a^2_{s_n\downarrow} \delta_{s_{n'\uparrow}} \\
&+ 2(1 + \cos\theta_{\nu} - \cos\theta_{\nu'} - \cos\theta_{\nu} \cos\theta_{\nu'}) a^2_{s_n\uparrow} \delta_{s_{n'\downarrow}})] \}
\end{aligned} \tag{20}$$

$$\begin{aligned}
\Delta Tr^{L}_{s_n, s_{n'}}(\theta_{\nu}, \theta_{\nu'}, \phi_{\nu'}) &= 32 E_{\nu} E_{\nu'} m_n^2 \, a_{s_n\uparrow} a_{s_n\downarrow} \{ C_V C_A \\
&\times [(\sin\theta_{\nu} (1 + \cos\theta_{\nu'}) + \sin\theta_{\nu'} (1 - \cos\theta_{\nu}) \cos\phi_{\nu'}) \delta_{s_{n'\uparrow}} \\
&+ (\sin\theta_{\nu} (1 - \cos\theta_{\nu'}) + \sin\theta_{\nu'} (1 + \cos\theta_{\nu}) \cos\phi_{\nu'}) \delta_{s_{n'\downarrow}}] \\
&+ C_A^2 \, [(\sin\theta_{\nu} (1 + \cos\theta_{\nu'}) - \sin\theta_{\nu'} (1 - \cos\theta_{\nu}) \cos\phi_{\nu'}) \delta_{s_{n'\uparrow}} \\
&+ (\sin\theta_{\nu} (1 - \cos\theta_{\nu'}) - \sin\theta_{\nu'} (1 + \cos\theta_{\nu}) \cos\phi_{\nu'}) \delta_{s_{n'\downarrow}}] \},
\end{aligned} \tag{21}$$

where

$$\cos\theta_{\nu,\nu'} = \cos\theta_{\nu} \cos\theta_{\nu'} + \sin\theta_{\nu} \sin\theta_{\nu'} \cos\phi_{\nu'}. \tag{22}$$

These expressions contain different kinds of quantum interference terms. In the first place, the terms proportional to the product $C_V C_A$ represent interference between the vector and axial-vector components of the weak interaction. These terms vanish in the absence of a magnetic field.

Our choice of the initial neutron wave function leads to two kinds of quantum interference terms from the hadron system: those proportional to $a^2_{s_n\downarrow} \delta_{s_{n'\uparrow}}$ or $a^2_{s_n\uparrow} \delta_{s_{n'\downarrow}}$, which we consider in this work; and those proportional to $a_{s_n\uparrow} a_{s_n\downarrow}$. The latter cancel out within our scheme but yield a non-zero contribution when correlations beyond the mean field are

taken into account. In our case, the strong interaction has been included at the mean-field level within the Hartree–Fock approximation in the equation of state (EoS). The implementation of higher-order correlations, such as the ring approximation (see, e.g., [50,51]), requires the inclusion of these terms.

We now return to Equation (13). Using momentum conservation, we performed the integration over $\vec{p}_{n'}$ and after some algebra we have

$$\frac{\sigma(p_\nu)}{V} = G_F^2 \int \frac{d\vec{p}_{\nu'}}{(2\pi)^3} \sum_{s_n, s_{n'}=\pm 1} Tr_{s_n, s_{n'}}(\theta_\nu, \theta_{\nu'}, \phi_{\nu'})\, S^0_{s_n, s_{n'}}(q_0, \vec{q}, T), \tag{23}$$

where $q_0 = E_\nu - E_{\nu'}$ and $\vec{q} = \vec{p}_\nu - \vec{p}_{\nu'}$. The structure function $S^0_{s_1, s_2}(q_0, \vec{q}, T)$, is defined by

$$S^0_{s_n, s_{n'}}(q_0, \vec{q}, T) = \frac{1}{(2\pi)^2} \int d\vec{p}_n\, \delta(q_0 + E_n - E_{n'})\, f_{s_n}(E_n, T)\, [1 - f_{s_{n'}}(E_{n'}, T)]. \tag{24}$$

An analytical expression for this function is given in the Appendix B. As we are considering massless neutrinos, $E_\nu = |\vec{p}_\nu|$.

Before concluding this section, we note that the limiting case $B \to 0$ is easily obtained from Equation (23) by setting $A_n = 0$, which leads to $a^2_{s_n\uparrow} = a^2_{s_n\downarrow} = 1/2$, and performing the spin summation. In this limit, the neutron single-particle energy becomes spin-independent. Consequently, the structure function is also spin-independent, and the spin summations in Equations (20) can be carried out straightforwardly.

4. Results and Discussion

In this section, we present our results for the neutrino and antineutrino mean free paths in hot, dense neutron matter under a strong magnetic field. We analyze a density range of $0.05 \leq \rho \leq 0.4$ fm^{-3}, several temperatures up to $T = 30$ MeV, and various magnetic field intensities ranging from $B = 0$ to $B = 10^{18}$ G. To describe the medium, we employ different models for the Equation of State (EoS) in order to assess the sensitivity of the mean free path to the properties of the medium. Most of the results are obtained using the LNS Skyrme interaction developed by Cao et al. [52], which we adopt because its particular density dependence of the effective mass makes it especially suitable for our framework. Unless otherwise specified, the equation of state just detailed is to be taken as the default model.

In all cases, neutrinos and antineutrinos are assumed to be massless and not trapped in the medium, so their chemical potential vanishes ($\mu_\nu = 0$). They are described by the standard Fermi–Dirac distribution,

$$f_{\nu,\bar{\nu}}(E_{\nu,\bar{\nu}}) = \frac{1}{e^{E_{\nu,\bar{\nu}}/T} + 1}, \tag{25}$$

with energy $E_{\nu,\bar{\nu}} = |\vec{p}_{\nu,\bar{\nu}}|$. Since $\mu_\nu = 0$, neutrinos and antineutrinos share the same distribution and energy for a given momentum. A representative value for their energy in a thermal medium is the average,

$$\langle E_{\nu,\bar{\nu}} \rangle = \frac{\int_0^\infty E^3/(e^{E/T}+1)\, dE}{\int_0^\infty E^2/(e^{E/T}+1)\, dE} = \frac{7\pi^4}{180\,\zeta(3)} T \approx 3.15\, T, \tag{26}$$

which corresponds to the thermal average energy of a relativistic fermion in equilibrium. However, for the sake of practicality and in line with common choices in the literature, we adopt the approximate value $E_{\nu,\bar{\nu}} = 3T$ in the following calculations. An immediate consequence of this approximation, considering that we explore temperatures starting from $T = 5$ MeV, is that the effect of the neutrino mass is negligible: the ratio $m_\nu/E_\nu \lesssim 6 \times 10^{-8}$.

It is worth noting that it is also possible to work at $T = 0$, but in that case, the neutrino energy must be modeled according to the emission mechanism. This conclusion is independent of the EoS, as it concerns the neutrino wave function, which does not enter into the EoS description.

Before discussing our results, it is worth noting that, for trapped neutrinos and antineutrinos, their distribution functions differ as follows:

$$f_\nu(E_\nu) = \frac{1}{e^{(E_\nu - \mu_\nu)/T} + 1}, \qquad f_{\bar{\nu}}(E_{\bar{\nu}}) = \frac{1}{e^{(E_{\bar{\nu}} + \mu_{\bar{\nu}})/T} + 1}. \tag{27}$$

This implies that $\langle E_\nu \rangle \neq \langle E_{\bar{\nu}} \rangle$, which would in turn lead to different mean free paths for neutrinos and antineutrinos. In addition, due to the definition of helicity, left-handed neutrinos and right-handed antineutrinos share the same analytical expression for the spinor (see Equations (A7) and (A9), respectively). Therefore, within our model, neutrinos and antineutrinos have identical mean free paths.

To begin the discussion of our results, we compare them with those previously obtained in Ref. [13], where certain approximations were made. Specifically, the neutron in the initial state was assumed to have either spin up or spin down. Furthermore, it was also assumed that the neutron's final state always retained the same spin orientation as the initial state. In our current model, the initial neutron spin state, given in Equation (A4), is a mixed state in which each spin component is weighted by a factor. These factors are chosen based on the results of the equation of state, so as to match the mean-field spin projection with the system's polarization. The use of such a wave function introduces quantum interference terms that allow for the initial and final neutron spin states to differ.

In Figure 1, we show the previous results (dashed lines) and compare them with those obtained using our improved scheme (solid lines). We recall that the $\hat{z}$-axis is defined along the direction of the constant magnetic field, thereby establishing a preferred spatial direction. In the absence of a magnetic field, the only relevant angle is the relative angle between the incoming and outgoing neutrino. In the presence of the field, however, we must consider the angle θ_ν between the initial neutrino direction and the magnetic field, the corresponding $\theta_{\nu'}$ for the outgoing neutrino, and the azimuthal angle $\phi_{\nu'}$ of the outgoing neutrino. The weak interaction dynamics lead to different values for the neutrino mean free path depending on θ_ν, as shown in Figure 1. This asymmetry in the mean free path suggests that, due to the scattering process, a higher number of neutrinos are expected to travel in the direction of the magnetic field, where the mean free path is longer.

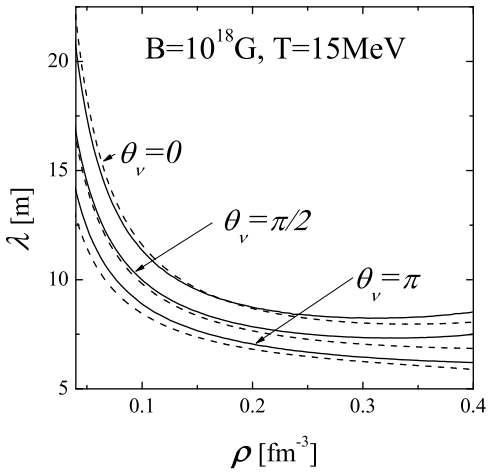

Figure 1. The Neutrino mean free path for two different models. The dashed lines correspond to the scheme in [13], while the solid lines represent the results of the present work. Both models were evaluated using the LNS Skyrme interaction [52].

Continuing with the discussion of Figure 1, we observe good consistency between both approximations. At low densities, the results for $\theta_\nu = \pi/2$ are very similar. For $\theta_\nu = 0$ and π, our present model shows a reduction in the asymmetry. The situation changes at higher densities: for all angles, the mean free path is longer in the present model. In any case, the differences between both models are noticeable. Two points should be emphasized: first, in Ref. [13], we noted that the results for $\theta_\nu = \pi/2$ were nearly identical for $B = 0$ and $B \neq 0$. This agreement remains valid in our improved model at low densities, but it no longer holds at high densities, where the mean free path increases compared to the previous model. Second, in this figure we have chosen a temperature of $T = 15$ MeV. This temperature smooths the results. We will later discuss the case of $T = 5$ MeV, which requires a more detailed analysis.

To enable a more quantitative analysis of these results, we define the function

$$\zeta = 100 \times \frac{\lambda - \lambda^{prev}}{\lambda^{prev}}, \tag{28}$$

where λ^{prev} denotes the neutrino mean free path obtained using the previous approximations from Ref. [13], and λ corresponds to the result from our improved model. Note that the mean free path depends functionally on ρ, T, B, and θ_ν, i.e., $\lambda = \lambda(\rho, T, B, \theta_\nu)$, although this dependence is omitted for brevity.

Table 1 presents the values of the function ζ for several densities and neutrino incident angles. This table supports the qualitative discussion given in Figure 1. Beyond the consistency between the two approximations, the differences introduced by the improved model are significant enough to justify its implementation. In particular, the value $\zeta = 9.65$ for $\rho/\rho_0 = 2.5$ and $\theta_\nu = \pi/2$ stands out. This result has important implications within our framework, although a detailed discussion is deferred to a later stage, specifically when analyzing the case of temperature $T = 5$ MeV. It is well understood that all models are approximations and inherently include some form of quantum interference terms. While our proposed model provides a more accurate treatment of certain quantum interference effects, direct comparisons between models remain challenging. Throughout this work, we somewhat arbitrarily use the term "interference term" as a shorthand to refer to our specific treatment of these terms.

Table 1. Values of the function ζ from Equation (28) for different densities and neutrino incident angles. The density is given in units of the saturation density, $\rho_0 = 0.16$ fm^{-3}. The EoS, temperature, and magnetic field strength are the same as in Figure 1.

ρ/ρ_0	$\theta_\nu = 0$	$\theta_\nu = \pi/2$	$\theta_\nu = \pi$
0.5	−2.97	1.81	6.01
1.0	−0.44	2.09	3.85
1.5	1.50	3.04	3.07
2.0	3.23	4.92	3.46
2.5	5.88	9.65	5.50

In what follows, we study the behavior of the neutrino mean free path as a function of the magnetic field strength, temperature, and the equation of state. We begin in Figure 2, showing results for different magnetic field strengths ranging from $B = 10^{15}$ G up to $B = 10^{18}$ G. For $\theta_\nu = \pi/2$ and at low densities, the results are nearly identical for all values of B (including $B = 0$). At high densities, we observe the previously mentioned increase in the mean free path for $B = 10^{18}$ G, which decreases with lower values of B and almost vanishes at $B = 10^{15}$ G. The asymmetry in the neutrino mean free path is significant for $B = 10^{18}$ G, barely noticeable for $B = 10^{17}$ G, and very small for the remaining values.

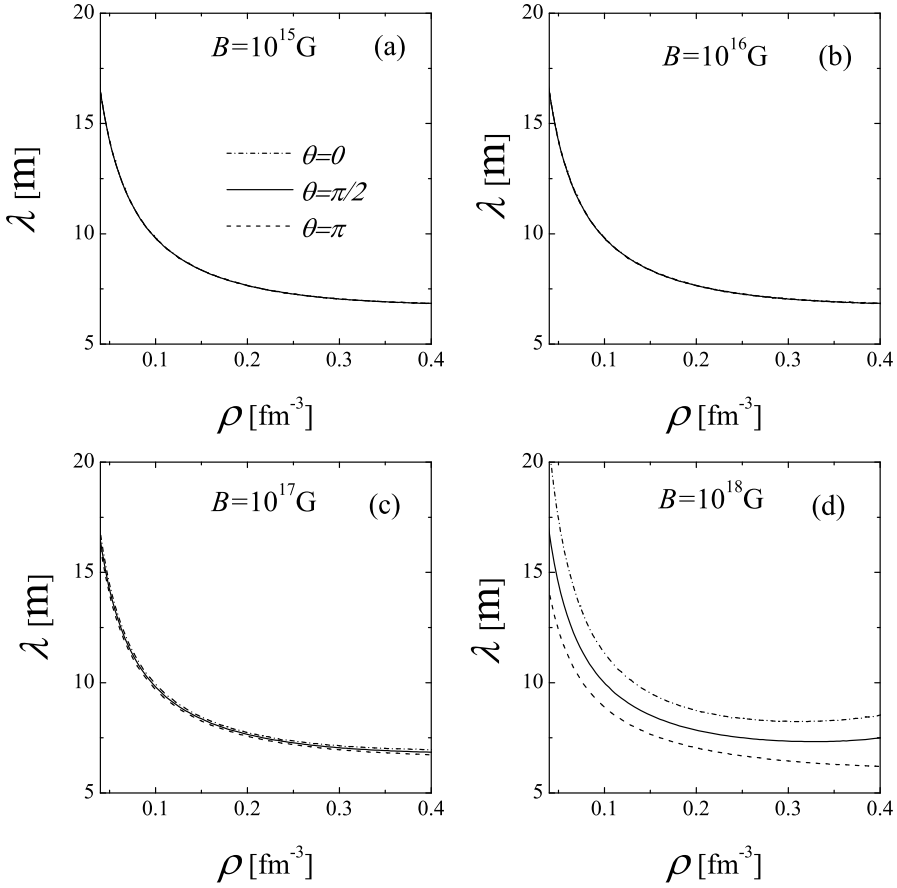

Figure 2. The Neutrino mean free path for different values of the magnetic field and for $T = 15$ MeV. The model interaction is the same as in Figure 1.

Next, in Figure 3, we analyze the effect of temperature on the neutrino mean free path. Recall that we evaluate the mean free path as the inverse of the total cross section per unit volume, as given by Equation (23). The available phase space is determined by the distribution functions $f_{s_n}(E_n, T)$ (see Equation (8)). As the temperature increases, these distribution functions allow access to a larger phase space, leading to an increase in the cross section and, consequently, a decrease in the mean free path, as shown in Figure 3. Regarding the asymmetry in the mean free path, it also decreases with increasing temperature (note the logarithmic scale in the figure). This is due to the reduction in spin polarization of the system at higher temperatures, which in turn leads to a reduced asymmetry in the mean free path. Thermal disorder tends to suppress spin alignment. Beyond these considerations, note the crossing of the mean free paths for $\theta_\nu = \pi/2$ and $\theta_\nu = 0$ at $T = 5$ MeV. This curious result is discussed in detail at the end of this section.

We now turn to the analysis of the dependence of the neutrino mean free path on different models for the equation of state (EoS). This study is performed using three EoS models: one that includes no strong interactions between neutrons, and two based on different parameterizations of the Skyrme-type effective interaction. The first is the LNS Skyrme model, and the second is the SLy4 model developed by Douchin et al. [53]. The Skyrme framework incorporates strong interactions at the mean-field level. In the absence of strong interactions, the EoS is determined solely by phase-space considerations arising from the Pauli exclusion principle. These three EoS models have been selected for the following reasons. The parameters of the LNS Skyrme model were fitted to reproduce the nuclear matter EoS obtained in the non-relativistic Brueckner–Hartree–Fock (BHF) approach using the Argonne V18 [54] nucleon–nucleon potential, supplemented with the Urbana IX [55] three-nucleon force. This model yields neutron effective masses that do

not deviate significantly from the bare mass; however, it exhibits a so-called ferromagnetic instability at high densities. In contrast, the SLy4 model does not present this issue, but it predicts small effective masses, which, as we will show, leads to an unexpected increase in the neutrino mean free path. Finally, the inclusion of an EoS without strong interactions serves to isolate and highlight the role of strong interactions in determining the neutrino mean free path. A similar analysis for charge-exchange reactions was presented in [56].

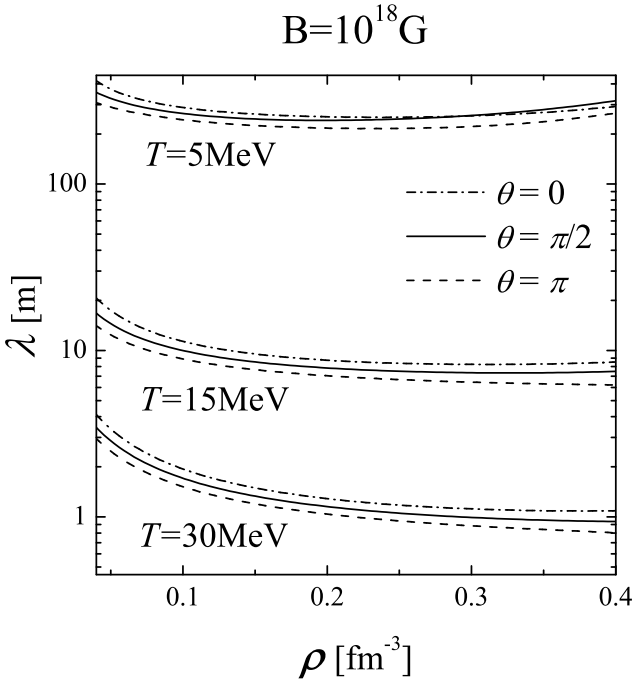

Figure 3. The Neutrino mean free path for different temperatures and for $B = 10^{18}$ G. The model interaction is the same as in Figure 1.

For convenience, we discuss this topic using two figures, Figures 4 and 5, corresponding to $T = 15$ MeV and $T = 5$ MeV, respectively. In both figures, panel (a) corresponds to the free (non-interacting) EoS, panel (b) to the LNS Skyrme model, and panel (c) to the Douchin parameterization of the strong interaction. From both figures, our first conclusion is that the neutrino mean free path shows a strong dependence on the EoS, as the results differ significantly across the various models. We emphasize this point, as our calculation is fully self-consistent: we compute the EoS, and from it, determine the spin asymmetry, the chemical potential, and the single-particle energies, which are then used in the calculation of the neutrino mean free path. To the best of our knowledge, there is no universally preferred set of EoS parameters. As a result, the predictions for the neutrino mean free path remain model-dependent, pending observational data that could provide constraints to select the most appropriate EoS.

We now examine the behavior of the neutrino mean free path in each panel individually. For simplicity, we focus on Figure 4 (the discussion for Figure 5 is very similar). The results for the free EoS shown in panel (a) illustrate the basic concepts of the problem: as the density increases, the probability of scattering events increases, and thus the mean free path decreases. Regarding the system's spin asymmetry, increasing the baryon density enhances the effect of the Pauli exclusion principle, favoring a more symmetric configuration with equal numbers of spin-up and spin-down particles. A direct consequence of this reduced spin asymmetry is a decrease in the asymmetry of the neutrino mean free path, as seen in panel (a).

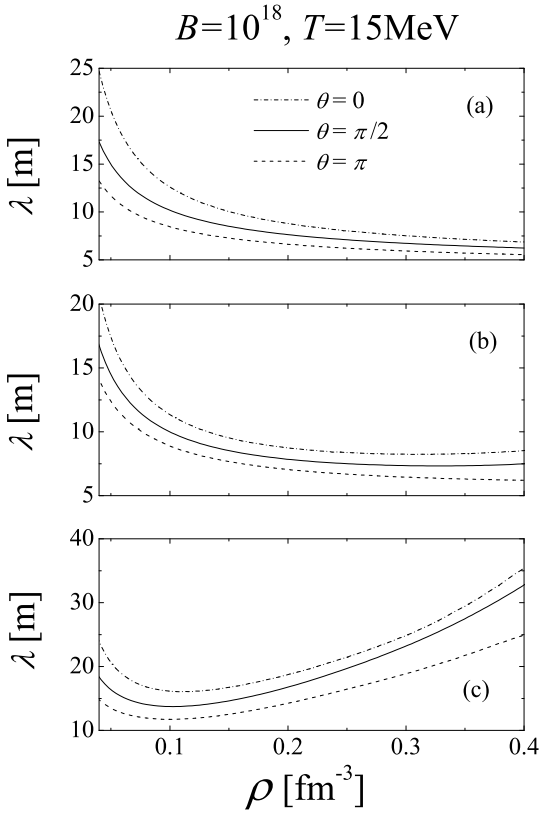

Figure 4. The Neutrino mean free path for different equations of state (EoSs), at $T = 15$ MeV and $B = 10^{18}$ G. In panel (**a**), the free interaction EoS is employed. Panels (**b**,**c**) use the Hartree–Fock approximation with Skyrme interactions. Specifically, panel (**b**) employs the LNS Skyrme interaction [52], while panel (**c**) uses the parameterization developed by Douchin et al. [53].

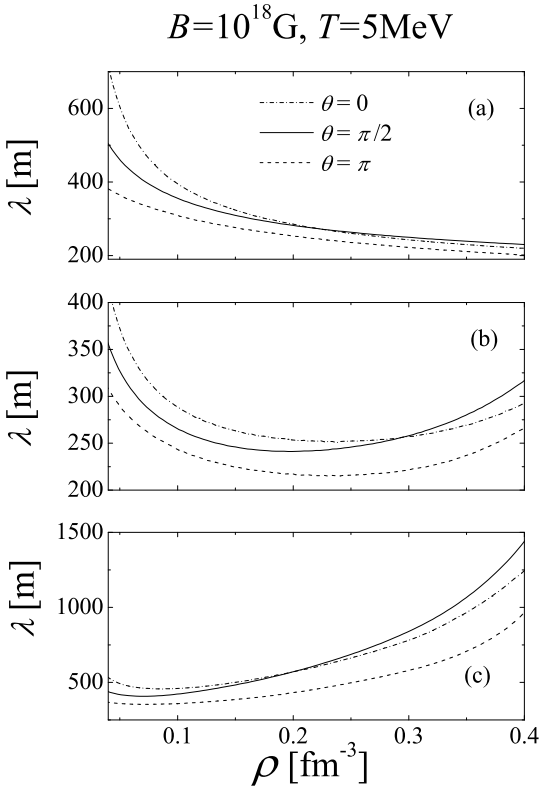

Figure 5. The The same as in Figure 4, but for $T = 5$ MeV. The meaning of each panel is the same as in Figure 4.

Panels (b) and (c) include the effects of the strong interaction, leading to a more complex behavior. At low densities, the (short-range) strong interaction plays a minor role, and the behavior resembles that of panel (a), albeit with a slightly reduced asymmetry in the mean free path. At higher densities, the strong interaction becomes more significant, and an increase in the mean free path with density is observed. This increase arises from two different effects. In particular, in panel (b), there is a non-physical magnetization of the system induced by the Skyrme interaction. Additionally, at high densities, a pronounced reduction in the neutron effective mass contributes to the increased mean free path; this effect is especially important in panel (c).

In both Figures 4 and 5, we observe an increase in the neutrino mean free path for $\theta_\nu = \pi/2$ relative to the two remaining angles. This effect is subtle at $T = 15$ MeV but becomes very pronounced at $T = 5$ MeV, where, in all panels, a crossing occurs with the result for $\theta_\nu = 0$. The origin of this behavior will be discussed in detail in the remainder of this section. From these figures, our first conclusion is that this feature is unlikely to be directly related to the EoS, as it appears consistently across all models considered.

The origin of the crossing of the mean free paths discussed above is subtle and involves several elements. It arises from quantum interference terms, which, to the best of our knowledge, are analyzed for the first time in the present work. These terms result from the dynamics of the weak interaction. At this stage, and for the purpose of gaining insight into the underlying mechanism, it is more convenient to consider the total cross section per unit volume rather than the mean free path. For simplicity, we focus on the free interaction EoS at $T = 5$ MeV. The total cross section is given in Equation (23) and can be naturally decomposed into four terms according to the spin projections of the initial and final neutron states: uu, ud, du, and dd. For instance, the ud term corresponds to an initial neutron with spin up and a final neutron with spin down. This decomposition is shown in Figure 6. All curves in panels (a) and (b) exhibit the expected behavior, namely a monotonic increase with density. What ultimately determines the behavior of the total cross section is the relative contribution of each term.

Panel (a) shows the sum of the direct contributions ($uu + dd$) and the interference terms ($ud + du$) for two relevant neutrino angles. All contributions increase monotonically with density. The direct terms converge at high densities, with $uu + dd$ taking consistently lower values for $\theta_\nu = 0$. The interference terms, on the other hand, behave differently: $ud + du$ is larger for $\theta_\nu = 0$ than for $\theta_\nu = \pi/2$, and the difference between the two remains approximately constant at medium and high densities. This panel reveals that the total contribution ($uu + dd + ud + du$) exhibits a crossing between the results for the two angles. This identifies the origin of the nontrivial behavior, though it does not yet constitute a full explanation. It is now clear that the interference terms are responsible for the observed feature. As already mentioned, to the best of our knowledge, these contributions are accounted for explicitly here for the first time.

We now turn to the trace function $Tr^{L}_{s_n,s_{n'}}(\theta_\nu, \theta_{\nu'}, \phi_{\nu'})$ in Equation (20). From this expression, we define two functions associated with the interference contributions:

$$\Theta_{ud}(\theta_\nu, \theta_{\nu'}) = 1 + \cos\theta_\nu - \cos\theta_{\nu'} - \cos\theta_\nu \cos\theta_{\nu'}, \quad (29)$$

$$\Theta_{du}(\theta_\nu, \theta_{\nu'}) = 1 - \cos\theta_\nu + \cos\theta_{\nu'} - \cos\theta_\nu \cos\theta_{\nu'}, \quad (30)$$

Inspection of Equation (20) shows that $\Theta_{ud}(\theta_\nu, \theta_{\nu'})$ and $\Theta_{du}(\theta_\nu, \theta_{\nu'})$ are associated with the ud and du contributions, respectively.

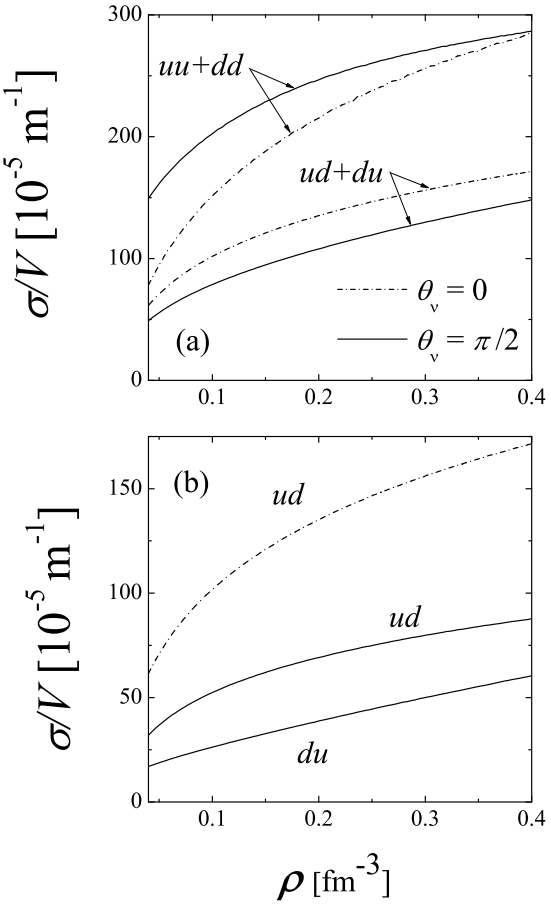

Figure 6. Different Contributions to the cross section per unit volume. The magnetic field intensity is $B = 10^{18}$ G and the temperature $T = 5$ MeV. Panel (**a**) shows the sum of the interference terms, while panel (**b**) displays the individual contribution of each term. Further details are provided in the main text.

Panel (b) of Figure 6 shows the individual interference terms. It is useful to keep in mind the expressions for Θ_{ud} and Θ_{du}, and their values for $\theta_\nu = 0$ and $\theta_\nu = \pi/2$, listed in Table 2. From this panel, one finds that

$$\begin{aligned} ud(\theta_\nu = 0) &\cong 2\, ud(\theta_\nu = \pi/2), \\ du(\theta_\nu = 0) &= 0, \end{aligned}$$

which can be directly understood from Table 2.

Table 2. Particular values for the functions $\Theta_{ud}(\theta_\nu, \theta_{\nu'})$ and $\Theta_{du}(\theta_\nu, \theta_{\nu'})$, as defined in Equations (29) and (30), respectively.

	$\boldsymbol{\theta_\nu = 0}$	$\boldsymbol{\theta_\nu = \pi/2}$	$\boldsymbol{\theta_\nu = \pi}$
$\Theta_{ud}(\theta_\nu, \theta_{\nu'})$	$2\,(1 - \cos\theta_{\nu'})$	$1 - \cos\theta_{\nu'}$	0
$\Theta_{du}(\theta_\nu, \theta_{\nu'})$	0	$1 + \cos\theta_{\nu'}$	$2\,(1 + \cos\theta_{\nu'})$

It remains to understand why $ud(\theta_\nu = \pi/2) > du(\theta_\nu = \pi/2)$. This result is somewhat counterintuitive, given that the system's polarization favors neutrons with spin down. In Equation (20), we observe that the ud contribution is weighted by the factor $a^2_{s_n\uparrow}$, while the corresponding factor for du is $a^2_{s_n\downarrow}$, with $a^2_{s_n\uparrow} < a^2_{s_n\downarrow}$. This inequality in the cross section can be understood in terms of the structure function $S^0_{s_1,s_2}(q_0, \vec{q}, T)$, defined in Equation (24). Figure 7 shows the structure function as a function of q_0 for a representative value of $|\vec{q}|$, selected from the numerical analysis.

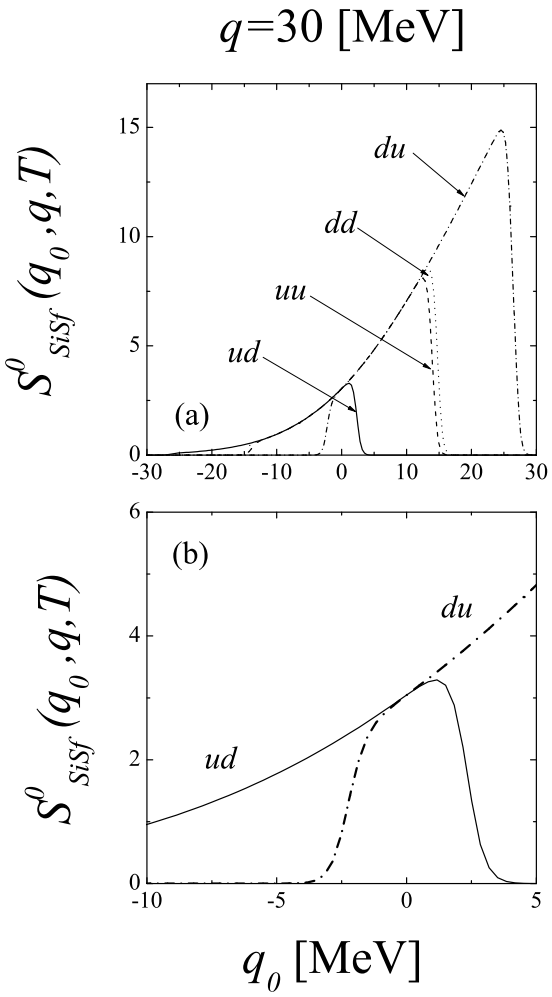

Figure 7. Energy Energy dependence of the structure function $S^0_{s_i,s_f}(q_0,q,T)$, shown in units of 10^{-3} MeV^{-1}fm^{-3}. The results correspond to a baryon density of $\rho/\rho_0 = 2.5$, where $\rho_0 = 0.16$ fm^{-3}. The spin projections s_i and s_f take the values u and d, corresponding to $s = 1$ and $s = -1$, respectively. The magnetic field strength is $B = 10^{18}$ G, and the temperature is fixed at $T = 5$ MeV. Panel (**a**) shows all the terms of the structure function, while panel (**b**) provides a detailed view of the interference terms of the same function.

Under the conditions of Figure 7 ($q = 30$ MeV), the cross section receives contributions from values of q_0 within the approximate range $\sim (-10, 5)$ MeV. These values are schematic in nature and are presented solely for illustrative purposes, to highlight the features of our results. Notably, over the entire range of q_0, S^0_{du} dominates over S^0_{ud}. However, due to the fixed neutrino energy $E_\nu = 3T$, the kinematics restrict the range of accessible q_0 values, as discussed above. This restriction accounts for the observed hierarchy between ud and du and also explains why the effect becomes less pronounced at higher temperatures.

In summary, the peculiar behavior originates in the weak interaction dynamics, encoded in the functions $\Theta_{ud}(\theta_\nu, \theta_{\nu'})$ and $\Theta_{du}(\theta_\nu, \theta_{\nu'})$. As a final point, in Figure 8, we present the neutrino mean free path as a function of the incoming neutrino angle θ_ν for two different baryon densities. At low density, the result is as expected: neutrinos are preferentially emitted parallel to the magnetic field. However, at high density, the maximum occurs near $\theta_\nu \lesssim \pi/2$. This outcome significantly alters the prevailing paradigm regarding asymmetric neutrino emission due to neutrino–neutron scattering. It indicates that at high densities and low temperatures, neutrinos are predominantly emitted perpendicular to the magnetic field. As discussed, this result is independent of the equation of state.

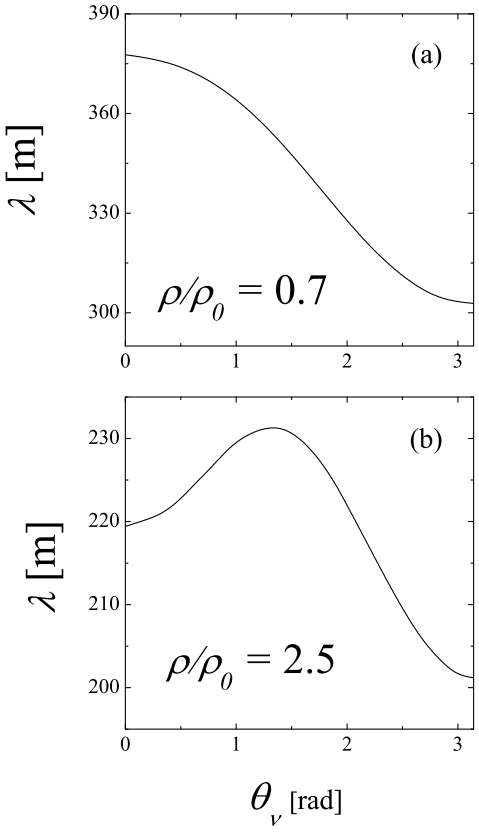

Figure 8. Neutrino Neutrino mean free path plotted as a function of the incoming neutrino angle θ_ν, over the interval $\theta_\nu \in [0, \pi]$, for two different baryon densities: $\rho/\rho_0 = 0.7$ in panel (**a**) and $\rho/\rho_0 = 2.5$ in panel (**b**). The magnetic field strength is $B = 10^{18}$ G, and the temperature is fixed at $T = 5$ MeV.

Before concluding this section, it is worth noting that, due to the scale of the reaction under consideration, the density, temperature, and magnetic field are treated as locally constant. In a realistic neutron star model, these quantities vary with position inside the star. To implement such a model, it is necessary to know the cross section (or, equivalently, the mean free path) for the reaction of interest, among other inputs; this is the focus of the present contribution. In a recent work [56], we addressed charge-exchange reactions under the same level of approximation. Unfortunately, our non-relativistic model is not suitable for describing the dense stellar core; a relativistic treatment is necessary. Together with the inclusion of nuclear correlations beyond the mean-field level, we consider the development of a relativistic model a possible direction for future work, although it lies beyond the scope of the present study. Under the conditions considered here, a fully relativistic model should reproduce our results in the appropriate limit. This highlights the role of the non-relativistic result as a guiding reference for the more comprehensive relativistic treatment.

Regarding the pulsar kick problem, our present results disfavor asymmetric neutrino emission as its explanation. This stands in contrast to the findings for charge-exchange reactions discussed in Ref. [56]. Ultimately, incorporating all relevant reactions into a realistic neutron star model would be necessary to resolve this issue conclusively. For a recent review of the pulsar kick problem, we refer the reader to the work of Lambiase and Poddar [57], where several possible explanations are briefly discussed.

5. Summary and Conclusions

In this work, we have analyzed the neutrino–neutron scattering reaction $\nu + n \to \nu' + n'$, in neutron matter at finite temperature and in the presence of a strong magnetic field. Particular attention was given to the issue of the neutrino mass, which remains an open

problem with far-reaching implications. Although our analysis shows that the inclusion of a finite neutrino mass does not affect the results presented here, this conclusion is nontrivial and, as such, warrants a dedicated discussion. The core of this study focused on the development and application of a formalism that explicitly includes quantum interference terms, which, to the best of our knowledge, had not been previously considered in this context. These interference terms were found to have a significant impact on the neutrino scattering process and, consequently, on the mean free path.

We performed a fully self-consistent calculation where the neutrino mean free path was computed using the same theoretical model as the equation of state (EoS), evaluated under identical conditions of density, temperature, and magnetic field. To assess the model dependence of the reaction rates, we also considered different EoSs. Our results show that the mean free path exhibits a strong sensitivity to the choice of EoS, underlining the relevance of adopting a self-consistent approach. The presence of the magnetic field introduces an angular asymmetry in the mean free path, which we have analyzed in detail. Remarkably, we find that the inclusion of quantum interference terms significantly alters the behavior of this asymmetry, modifying the prevailing paradigm that has governed our understanding of neutrino–neutron scattering in magnetized matter up to now. Furthermore, we observe that for low and intermediate densities, the neutrino flux is enhanced for neutrinos propagating parallel to the magnetic field. In contrast, at high densities, the dominant contribution to the flux arises from neutrinos moving perpendicular to the field. Assuming that the magnetic field of the star possesses cylindrical symmetry, the emission of neutrinos in the direction perpendicular to the field results in a significant suppression of the relative weight of this contribution to the explanation of the pulsar kick phenomenon.

As discussed in the previous paragraph, quantum interference terms play a crucial role not so much in determining the mean free path itself, but rather in modifying its angular dependence. These terms are included for the first time in this work and originate from a dynamical effect of the weak interaction. Remarkably, we find that this effect persists across all the EoS models considered. The strong interaction is treated at the mean-field level throughout our analysis. However, we also show that going beyond the mean-field approximation leads to the emergence of a new set of interference terms, which have not been previously explored. In this work, we provide the analytical expressions for these additional contributions. Their impact could be further investigated by incorporating correlations of the ring type, which offers a promising direction for future studies.

Author Contributions: Conceptualization and Formalism: E.B. Numerical Analysis and Discussion: E.B. and V.D.O. All authors have read and agreed to the published version of the manuscript.

Funding: This research received no external funding.

Data Availability Statement: The original contributions presented in this study are included in the article. Further inquiries can be directed to the corresponding author.

Acknowledgments: We thank O. Civitarese and A. Szynkman for the fruitful discussions. E. B. is a member of the Carrera del Investigador Científico of the Consejo Nacional de Investigaciones Científicas y Técnicas (CONICET), Argentina.

Conflicts of Interest: The authors declare no conflicts of interest.

Appendix A. Wave Function for Neutrons, Neutrinos, and Antineutrinos

This appendix is devoted to the description of the wave functions for the neutron and the neutrino. All wave functions are normalized within a reference volume V, introduced for convenience. It is important to note that the final expressions for the cross section per unit volume do not depend on the specific choice of V. We assume a uniform magnetic

field oriented along the z-axis, $\mathbf{B} = B\hat{k}$. Furthermore, as noted in the main body of the text, a distinction is made between wave functions corresponding to the initial and final states.

Appendix A.1. The Neutron

We employ a non-relativistic wave function for the neutron, given by

$$\Psi_n(\vec{r},t) = (V)^{-1/2} e^{i(\vec{p}_n\cdot\vec{r}-E_n t)}\; U_n, \tag{A1}$$

where

$$E_n = m_n + \frac{p_n^2}{2m_{s_n}^*} + \frac{v_{s_n}}{8} - s_n \mu_{Bn} B, \tag{A2}$$

with $\mu_{Bn} = -1.913\mu_N$. In this expression, $m_{s_n}^*$ represents the effective mass, and v_{s_n} denotes the single-particle energy potential. Both quantities depend on spin, and their analytical expressions within the Skyrme model can be found in [46,58]. For the non-interacting model, we have $m_{s_n}^* \to m_n$ and $v_{s_n} \to 0$.

For the spin part of the wave function, we distinguish between the neutron being in the initial or final state:

i. Neutron in the initial state: The spin component of the wave function is given by

$$U_n \;=\; (a_{n\uparrow}) \begin{pmatrix} 1 \\ 0 \\ 0 \\ 0 \end{pmatrix} + (a_{n\downarrow}) \begin{pmatrix} 0 \\ 1 \\ 0 \\ 0 \end{pmatrix}. \tag{A3}$$

ii. Neutron in the final state: We have two spinors

$$U_{s_{n'}} \;=\; \begin{pmatrix} \delta_{s_{n'}\uparrow} \\ \delta_{s_{n'}\downarrow} \\ 0 \\ 0 \end{pmatrix}, \tag{A4}$$

and we must sum up over $s_n = +/-1$, for spin up or down, respectively. Finally, at this point, it is convenient to include

$$\int d\Pi_n \;=\; \sum_{s_n=\pm 1} \frac{1}{(2\pi)^3} \int d^3 p_n. \tag{A5}$$

Appendix A.2. The Neutrino

We are considering massless neutrinos which are left-handed (or polarized). In this case, for a neutrino with momentum $\vec{p}_\nu$, its energy is $\mid \vec{p}_\nu \mid$ and the wave function is given by

$$\Psi_\nu^L(\vec{r},t) = V^{-1/2} e^{i(\vec{p}_\nu\cdot\vec{r}-|\vec{p}_\nu|t)}\; U_\nu^L(\theta_\nu,\phi_\nu), \tag{A6}$$

where

$$U_\nu^L(\theta_\nu,\phi_\nu) \;=\; \frac{1}{\sqrt{2}} \begin{pmatrix} -\sqrt{1-\cos(\theta_\nu)}\, e^{-i\phi_\nu} \\ \sqrt{1+\cos(\theta_\nu)} \\ \sqrt{1-\cos(\theta_\nu)}\, e^{-i\phi_\nu} \\ -\sqrt{1+\cos(\theta_\nu)} \end{pmatrix}, \tag{A7}$$

where θ_ν is the polar angle for $\vec{p}_\nu$ and ϕ_ν is its azimuthal angle. As we are considering a single neutrino with its wave function given by Equation (A6), no summation over the neutrino initial state is needed.

Appendix A.3. The Antineutrino

The massless antineutrinos are right-handed. The wave function is given by

$$\Psi_{\bar{\nu}}(\rho, \phi_{\bar{\nu}}, z, t) = V^{-1/2} e^{-i(\vec{p}_{\bar{\nu}} \cdot \vec{r} - |\vec{p}_{\bar{\nu}}| t)} \, U_{\bar{\nu}}(\theta_{\bar{\nu}}, \phi_{\bar{\nu}}), \tag{A8}$$

where $\vec{p}_{\bar{\nu}}$ is the momentum, $\mid \vec{p}_{\bar{\nu}} \mid$ its energy, and

$$U_{\bar{\nu}}(\theta_{\bar{\nu}}, \phi_{\bar{\nu}}) \;=\; \frac{1}{\sqrt{2}} \begin{pmatrix} -\sqrt{1-\cos(\theta_{\bar{\nu}})}\, e^{-i\phi_{\bar{\nu}}} \\ \sqrt{1+\cos(\theta_{\bar{\nu}})} \\ \sqrt{1-\cos(\theta_{\bar{\nu}})}\, e^{-i\phi_{\bar{\nu}}} \\ -\sqrt{1+\cos(\theta_{\bar{\nu}})} \end{pmatrix}, \tag{A9}$$

is the antineutrino spinor, where $\theta_{\bar{\nu}}$ is the polar angle of $\vec{p}_{\bar{\nu}}$, and $\phi_{\bar{\nu}}$ is its azimuthal angle. Note that massless neutrinos are left-handed, while antineutrinos are right-handed. The helicity operator differs in sign due to the momentum of these particles, which explains why Equations (A7) and (A9) are identical. Additionally, since massless neutrinos and antineutrinos have only one possible state, there is no need to distinguish between initial and final states.

Appendix B. Evaluation of the Structure Function S^0

In this Appendix, we derive an analytical expression for the structure function of a system of neutral particles in a strong magnetic field. A similar derivation, but for unpolarized particles, can be found in [23]. We provide the most general expression for this structure function. The structure function is given by the following expression:

$$S^0_{s_1,s_2}(q_0, \vec{q}, T) = \frac{1}{(2\pi)^2} \int d\vec{p}_1 \, \delta(q_0 + E_1 - E_2) \, f_1(E_1, T) \, [1 - f_2(E_2, T)], \tag{A10}$$

where $\vec{p}_1$ is the momentum of the hadron in the initial state. For the final state, we have $\vec{p}_2 = \vec{p}_1 + \vec{q}$. The distribution function is given by

$$f_{s_i}(E_i, T) = \frac{1}{1 + e^{(E_i - \mu_i)/T}}. \tag{A11}$$

For neutral particles within the Skyrme model, the single-particle energy is given by the following:

$$E_1 \;=\; m_N + \frac{p_1^2}{2m^*_{s_1}} + \frac{v_{s_1}}{8} - s_1 \mu_{Bn} B, \tag{A12}$$

$$E_2 \;=\; m_N + \frac{(\vec{p}_1 + \vec{q})^2}{2m^*_{s_2}} + \frac{v_{s_2}}{8} - s_2 \mu_{Bn} B, \tag{A13}$$

where m_N is the nucleon mass. In this expression, the effective mass ($m^*_{s_i}$), together with the single particle potential energy (v_{s_i}), depend on the density of the system, and explicit expressions are found in [46,58]. To solve the integral in Equation (A10), we start analyzing the energy coacervation:

$$q_0 + E_1 - E_2 = 0, \tag{A14}$$

where we now employ the expressions for E_1 and E_2 given in Equations (A12) and (A13), respectively. After some algebra, we found

$$\kappa_0 = \frac{m^*_{s_2}}{p_1 q}\left(\Delta_M\, p_1^2 + \omega_0 - \frac{q^2}{2m^*_{s_2}}\right), \tag{A15}$$

with the following definitions:

$$\begin{aligned} \kappa &= \frac{\vec{p}_1 \cdot \vec{q}}{p_1 q}, \\ \omega_0 &= q_0 + \frac{1}{8}\left(v_{s_1} - v_{s_2}\right) + (s_2 - s_1)\mu_{Bn} B, \\ \Delta_M &= \frac{1}{2}\left(\frac{1}{m^*_{s_1}} - \frac{1}{m^*_{s_2}}\right). \end{aligned} \tag{A16}$$

Now the energy conservation is rewritten as

$$\delta(q_0 + E_1 - E_2) = \frac{m^*_{s_2}}{p_1 q}\,\delta(\kappa - \kappa_0). \tag{A17}$$

Considering that

$$\int d\vec{p}_1 = \int_0^{2\pi} d\phi \int_{-1}^{1} d\kappa \int_0^{\infty} dp_1\, p_1^2, \tag{A18}$$

and using the energy conservation, Equation (A10) is now

$$S^0_{s_1,s_2}(q_0, \vec{q}, T) = \frac{1}{2\pi}\frac{m^*_{s_2}}{q}\int_{|\kappa_0|\leq 1} dp_1\, p_1\;\; f_1(E_1, T)\,[1 - f_2(E_1 + q_0, T)]. \tag{A19}$$

To solve this integral, we define

$$\begin{aligned} \xi &= \frac{E_1 - \mu_1}{T} \\ \zeta &= \frac{q_0 + \mu_1 - \mu_2}{T}, \end{aligned} \tag{A20}$$

we have $dp_1\, p_1 = T m^*_{s_1} d\xi$. After some algebra, we rewrite Equation (A19) as

$$\begin{aligned} S^0_{s_1,s_2}(q_0, \vec{q}, T) &= \frac{1}{2\pi}\frac{m^*_{s_1} m^*_{s_2}\, T}{q}\int d\xi\;\; \frac{1}{1 + e^{\xi}}\;\frac{1}{1 + e^{-\xi-\zeta}}, \\ &= \frac{1}{2\pi}(-1)\,\frac{m^*_{s_1} m^*_{s_2}\, T}{q}\;\; \frac{1}{1 - e^{-\zeta}}\;\ln\frac{1 + e^{\xi}}{e^{-\zeta} + e^{\xi}}\Bigg|_{(p_1)_{min}}^{(p_1)_{max}}. \end{aligned} \tag{A21}$$

This is the final expression for the structure function after fixing the integration limits, $(p_1)_{min}$ and $(p_1)_{max}$. These values are determined by the condition $|\kappa_0| \leq 1$, and after squaring Equation (A15), we obtain the following:

$$f(x) \equiv \alpha\, x^2 + \beta\, x + \gamma \leq 0, \tag{A22}$$

where

$$\begin{aligned} x &= p_1^2, \\ \alpha &= \Delta_M^2, \\ \beta &= 2\Delta_M\left(\omega_0 - \frac{q^2}{2m^*_{s_2}}\right) - \left(\frac{q}{m^*_{s_2}}\right)^2, \\ \gamma &= \left(\omega_0 - \frac{q^2}{2m^*_{s_2}}\right)^2. \end{aligned} \tag{A23}$$

The roots of Equation (A22), together with the condition $f(x) \leq 0$, determine the range of integration. In the following, we analyze the two possible cases according to the relative values of the masses.

Appendix B.1. When $m^*_{s_1} \neq m^*_{s_2}$

This situation take place when $s_1 \neq s_2$, and also when we have two different kind of particles. Note that by construction, $\alpha \geq 0$. The range of integration is obtain by the roots of $f(x) = 0$. Let us call these roots x_{min} and x_{max}, with $x_{min} \leq x_{max}$. To analyze the different possibilities, we introduce

$$disc \equiv \beta^2 - 4\,\alpha\,\gamma.$$

Having in mind the condition $f(x) \leq 0$, we have

- If $disc < 0$, then $S^0(q_0, \vec{q}, T) = 0$, because the condition $f(x) \leq 0$ can not be fulfilled.
- If $disc = 0$, then $S^0(q_0, \vec{q}, T) = 0$ because there is only one point where the condition $f(x) \leq 0$ is fulfilled.
- If $disc > 0$ and $x_{max} \leq 0$, then $S^0(q_0, \vec{q}, T) = 0$ because there are no real values for p_1.
- If $disc > 0$ and $x_{min} \leq 0$, but $x_{max} > 0$, then the integration over p_1 has the range $p_1 \in [0, \sqrt{x_{max}}]$.
- If $disc > 0$ and $x_{min} \geq 0$, then the integration over p_1 has the range $p_1 \in [\sqrt{x_{min}}, \sqrt{x_{max}}]$.

Appendix B.2. When $m^*_{s_1} = m^*_{s_2}$

In this case, $\Delta_M = 0$, and Equation (A22) reduces to

$$\beta\, x + \gamma \leq 0, \tag{A24}$$

therefore, the limits of integration are

$$\begin{aligned} (p_1)_{min} &= \frac{m^*_{s_2}\omega_0}{q} - \frac{q}{2}, \\ (p_1)_{max} &\rightarrow \infty, \end{aligned} \tag{A25}$$

References

1. Fukuda, Y.; Hayakawa, T.; Ichihara, E.; Inoue, K.; Ishihara, K.; Ishino, H.; Itow, Y.; Kajita, T.; Kameda, J.; Kasuga, S.; et al. Evidence for Oscillation of Atmospheric Neutrinos. *Phys. Rev. Lett.* **1998**, *81*, 1562–1567. [CrossRef]
2. Duncan, R.C.; Thompson, C. Formation of Very Strongly Magnetized Neutron Stars: Implications for Gamma-Ray Bursts. *Astrophys. J.* **1992**, *392*, L9–L13. [CrossRef]
3. Yakovlev, D.G.; Gnedin, O.Y.; Kaminker, A.D.; Levenfish, K.P.; Potekhin, A.Y. Neutron Star Cooling: Theoretical Aspects and Observational Constraints. *Adv. Space Res.* **2004**, *33*, 523–530. [CrossRef]
4. Burrows, A.; Vartanyan, D. Core-collapse supernova explosion theory. *Nature* **2021**, *589*, 29–39. [CrossRef]
5. Ferrer, E.J.; de la Incera, V. Neutrino Propagation and Oscillations in a Strong Magnetic Field. *Int. J. Mod. Phys. A* **2004**, *19*, 5385–5393. [CrossRef]
6. Popov, A.; Studenikin, A. Neutrino Eigenstates and Flavour, Spin and Spin-Flavour Oscillations in a Constant Magnetic Field. *Eur. Phys. J. C* **2019**, *79*, 144. [CrossRef]
7. Grigoriev, A.; Kupcheva, E.; Ternov, A. Neutrino spin oscillations in polarized matter. *Phys. Lett. B* **2019**, *797*, 134861. [CrossRef]
8. Sasaki, H.; Takiwaki, T. Neutrino-antineutrino oscillations induced by strong magnetic fields in dense matter. *Phys. Rev. D* **2021**, *104*, 023018. [CrossRef]
9. Tamborra, I.; Hanke, F.; Janka, H.T.; Müller, B.; Raffelt, G.G.; Marek, A. Neutrino Emission Characteristics and Detection Opportunities Based on Three-Dimensional Supernova Simulations. *Phys. Rev. D* **2014**, *90*, 045032. [CrossRef]
10. Hobbs, G.; Lorimer, D.R.; Lyne, A.G.; Kramer, M. A Statistical Study of 233 Pulsar Proper Motions. *Mon. Not. R. Astron. Soc.* **2005**, *360*, 974–992. [CrossRef]
11. Lai, D.; Qian, Y.Z. Neutrino Transport and Pulsar Kicks: The Role of Asymmetric Magnetic Fields. *Astrophys. J.* **1998**, *505*, 844–853. [CrossRef]

12. Arras, P.; Lai, D. Neutrino-nucleon interactions in protoneutron stars: The effect of parity violation. *Astrophys. J.* **1999**, *519*, 745–753. [CrossRef]
13. Patiño, J.T.; Bauer, E.; Vidaña, I. Asymmetry of the neutrino mean free path in hot neutron matter under strong magnetic fields. *Phys. Rev. C* **2019**, *99*, 045808. [CrossRef]
14. Tubbs, D.L.; Schramm, D.N. Neutrino opacities at high temperatures and densities. *Astrophys. J.* **1975**, *201*, 467–488. [CrossRef]
15. Sawyer, R.F. Neutrino opacity of neutron-star matter. *Phys. Rev. D* **1975**, *11*, 2740–2745. [CrossRef]
16. Iwamoto, N.; Pethick, C.J. Effects of nucleon-nucleon interactions on scattering of neutrinos in neutron matter. *Phys. Rev. D* **1982**, *25*, 313–329. [CrossRef]
17. Bäckman, S.O.; Källman, C.G.; Sjöberg, O. Nucleon-nucleon interactions and nuclear matter properties. *Phys. Lett. B* **1973**, *43*, 263–266. [CrossRef]
18. Haensel, P.; Jerzak, A.J. Mean free paths of non-degenerate neutrinos in neutron star matter. *Astron. Astrophys.* **1987**, *179*, 127–133.
19. Reddy, S.; Prakash, M.; Lattimer, J.M.; Pons, J.A. Effects of strong and electromagnetic correlations on neutrino opacities in dense matter. *Phys. Rev. C* **1999**, *59*, 2888–2918. [CrossRef]
20. Horowitz, C.J.; Wehrberger, K. Neutrino neutral current interactions in nuclear matter. *Nucl. Phys. A* **1991**, *531*, 665–684. [CrossRef]
21. Reddy, S.; Prakash, M. Neutrino scattering in a newly born neutron star. *Astrophys. J.* **1997**, *478*, 689–700. [CrossRef]
22. Reddy, S.; Prakash, M.; Lattimer, J. Neutrino interactions in hot and dense matter. *Phys. Rev. D* **1998**, *58*, 013009. [CrossRef]
23. Reddy, S. Neutrino Interactions in Hot and Dense Matter. Ph.D. Thesis, State University of New York at Stony Brook, New York, NY, USA, 1998.
24. Burrows, A.; Sawyer, R. The effects of correlations on neutrino opacities in nuclear matter. *Phys. Rev. C* **1998**, *58*, 554. [CrossRef]
25. Navarro, J.; Hernández, E.S.; Vautherin, D. Medium effects in neutrino scattering off nucleons. *Phys. Rev. C* **1999**, *60*, 045801. [CrossRef]
26. Shen, C.; Lombardo, U.; Giai, N.V.; Zuo, W. Nuclear matter response functions with effective interactions. *Phys. Rev. C* **2003**, *68*, 055802. [CrossRef]
27. Margueron, J.; Vidaña, I.; Bombaci, I. Superfluid effects on neutrino mean free paths in neutron stars. *Phys. Rev. C* **2003**, *68*, 055806. [CrossRef]
28. Bezchastnov, V.G.; Haensel, P. Neutrino scattering in neutron-star crusts. *Phys. Rev. D* **1996**, *54*, 3706. [CrossRef]
29. Kusenko, A.; Segrè, G. Pulsar kicks from neutrino oscillations. *Phys. Rev. Lett.* **1996**, *77*, 4872. [CrossRef]
30. Horowitz, C.J.; Li, G. Neutral-current neutrino interactions in supernovae. *Phys. Rev. Lett.* **1998**, *80*, 3694. [CrossRef]
31. Baiko, D.A.; Yakovlev, D.G. Thermal conductivity of neutrons in neutron star cores. *Astron. Astrophys.* **1999**, *342*, 192. [CrossRef]
32. Arras, P.; Lai, D. Neutrino-nucleon scattering in magnetized proto–neutron stars. *Phys. Rev. D* **1999**, *60*, 043001. [CrossRef]
33. Chandra, D.; Goyal, A.; Goswami, K. Neutrino interactions in a strongly magnetized dense medium. *Phys. Rev. D* **2002**, *65*, 053003. [CrossRef]
34. Ando, S. Nonradiative neutrino decay and supernova neutrino signals. *Phys. Rev. D* **2003**, *68*, 063002. [CrossRef]
35. Horowitz, C.J.; Schwenk, A. Neutrino-nucleon scattering in supernova matter from the virial expansion. *Phys. Lett. B* **2006**, *642*, 326. [CrossRef]
36. Sagert, I.; Schaffner-Bielich, J. Signals of the QCD phase transition in core-collapse supernovae. *Astron. Astrophys.* **2008**, *489*, 281. [CrossRef]
37. Pérez-García, M.A. Neutrino propagation in magnetized neutron matter. *Phys. Rev. C* **2009**, *80*, 045804. [CrossRef]
38. Pérez-García, M.A. Effect of magnetic fields on neutrino propagation in neutron matter. *Eur. Phys. J. A* **2010**, *44*, 77.
39. Bauer, E.; Patiño, J.T. Neutrino mean free path in neutron star matter with Skyrme interactions and tensor force. *Phys. Rev. C* **2020**, *101*, 065806. [CrossRef]
40. Bauer, E.; Patiño, J.T.; Benvenuto, O.G. Neutrino mean free paths in hot and dense matter revisited. *Phys. Rev. C* **2023**, *107*, 065804. [CrossRef]
41. Schechter, J.; Valle, J.W.F. Neutrino masses in SU(2)×U(1) theories. *Phys. Rev. D* **1981**, *24*, 1883. [CrossRef]
42. Akhmedov, E.K. Resonant amplification of neutrino spin rotation in matter and the solar-neutrino problem. *Phys. Lett. B* **1988**, *213*, 64. [CrossRef]
43. Lim, C.S.; Marciano, W.J. Resonant spin-flavor precession of neutrinos in matter. *Phys. Rev. D* **1988**, *37*, 1368. [CrossRef] [PubMed]
44. Giunti, C.; Kim, C.W. *Fundamentals of Neutrino Physics and Astrophysics*; Oxford University Press: Oxford, UK, 2007.
45. Vautherin, D.; Brink, D.M. Hartree-Fock calculations with Skyrme's interaction. I. Spherical nuclei. *Phys. Rev. C* **1972**, *5*, 626. [CrossRef]
46. Aguirre, R.; Bauer, E.; Vidaña, I. Medium modifications of the nucleon effective mass and neutrino mean free path. *Phys. Rev. C* **2014**, *89*, 035809. [CrossRef]
47. Benvenuto, O.G.; Bauer, E.; Vidaña, I. Mean free path of neutrinos in neutron-star matter using Skyrme interactions. *Eur. Phys. J. A* **2023**, *59*, 159. [CrossRef]

48. Joachin, C.J. *Quantum Collision Theory*; North-Holland Publishing Company: Amsterdam, The Netherland, 1975.
49. Duan, H.; Qian, Y.Z. Collective neutrino flavor transformation in supernovae. *Phys. Rev. D* **2005**, *72*, 023005. [CrossRef]
50. Roberts, L.F.; Reddy, S. Charged-current neutrino interactions in hot and dense matter. *Phys. Rev. C* **2017**, *95*, 045807. [CrossRef]
51. Roberts, L.F.; Reddy, S.; Shen, G. Medium modification of the charged-current neutrino opacity and its implications. *Phys. Rev. C* **2012**, *86*, 065803. [CrossRef]
52. Cao, L.G.; Lombardo, U.; Shen, C.W.; Giai, N.V. Effective mass in nuclear matter with realistic nucleon-nucleon interactions. *Phys. Rev. C* **2006**, *73*, 014313. [CrossRef]
53. Douchin, F.; Haensel, P.; Meyer, J. Inner edge of neutron-star crust. *Nucl. Phys. A* **2000**, *665*, 419. [CrossRef]
54. Wiringa, R.B.; Stoks, V.G.J.; Schiavilla, R. Accurate nucleon-nucleon potential with charge-independence breaking. *Phys. Rev. C* **1995**, *51*, 38–51. [CrossRef] [PubMed]
55. Pudliner, B.S.; Pandharipande, V.R.; Carlson, J.; Wiringa, R.B. Quantum Monte Carlo Calculations of $A \leq 6$ Nuclei. *Phys. Rev. Lett.* **1995**, *74*, 4396–4399. [CrossRef] [PubMed]
56. Bauer, E.; Patiño, J.T. Absorption and emission of neutrinos and antineutrinos in hot stellar matter with a strong magnetic field. *Phys. Rev. C* **2025**, *111*, 055802. [CrossRef]
57. Lambiase, G.; Poddar, T.K. Pulsar Kick: Status and Perspective. *Symmetry* **2024**, *16*, 1649. [CrossRef]
58. Aguirre, R. Superfluid neutron matter and neutrino emissivity. *Phys. Rev. C* **2011**, *83*, 055804. [CrossRef]